Modelling of light-induced chlorophyll *a* fluorescence rise (O-J-I-P transient) and changes in 820 nm-transmittance signal of photosynthesis

D. LAZÁR[*,**]

Laboratory of Biophysics, Faculty of Science, Palacký University, Tř. Svobody 26, 771 46 Olomouc, Czech Republic[*]
Photon Systems Instruments, Ltd., Koláčkova 39, 621 00 Brno, Czech Republic[**]

Abstract

Theoretical modelling is often overlooked in photosynthesis research even if it can significantly help with understanding of explored system. A new model of light-induced photosynthetic reactions occurring in and around thylakoid membrane is introduced here and used for theoretical modelling of not only the light-induced chlorophyll (Chl) *a* fluorescence rise (FLR; the O-J-I-P transient), reflecting function of photosystem II (PSII), but also of the 820 nm-transmittance signal (I_{820}), reflecting function of photosystem I (PSI) and plastocyanin (PC), paralleling the FLR. Correctness of the model was verified by successful simulations of the FLR and I_{820} signal as measured with the control (no treatment) sample but also as measured with 2,5-dibromo-3-methyl-6-isopropyl-p-benzoquinone- (inhibits electron transport in cytochrome b_6/f) and methylviologen- (accepts electrons from iron-sulphur cluster of PSI) treated samples and with the control sample upon different intensities of excitation light. From the simulations performed for the control sample, contribution of the oxidised donor of PSI, P700, and oxidised PC to the I_{820} signal minimum (reflects maximal accumulations of the two components) was estimated to be 75% and 25%, respectively. Further in silico experiments showed that PC must be reduced in the dark, cyclic electron transport around PSI must be considered in the model and activation of ferredoxin-$NADP^+$-oxidoreductase (FNR) also affects the FLR. Correct simulations of the FLR and I_{820} signal demonstrate robustness of the model, confirm that the electron transport reactions occurring beyond PSII affect the shape of the FLR, and show usefulness and perspective of theoretical approach in studying of the light-induced photosynthetic reactions.

Additional key words: cytochrome b_6/f; ferredoxin-$NADP^+$-oxidoreductase, photosystem I; photosystem II; theory.

Introduction

As photosynthesis is one of the most important biological processes occurring on the Earth, a detailed understanding of the photosynthetic processes is very important and needed. To access photosynthetic function, measurement of chlorophyll (Chl) *a* fluorescence by different techniques is very often used. One of the techniques is Chl *a* fluorescence induction (FLI) which is measurement of time course of fluorescence signal during illumination of a dark-adapted photosynthetic sample. Measurement of FLI is attractive because it is non-invasive, fast, and easy, it is inexpensive, and above all it provides access to a range of processes that play a role in

Received 22 May 2009, *accepted* 24 September 2009.
Fax: +420-58-5225737, email: lazard@seznam.cz
Abbreviations: b_H or H – high potential haem *b* of cyt b_6/f; b_L or L – low potential haem *b* of cyt b_6/f; *c* or C – haem *c* of cyt b_6/f; CET – cyclic electron transport; Chl – chlorophyll; cyt – cytochrome; DBMIB – 2,5-dibromo-3-methyl-6-isopropyl-p-benzoquinone; F – haem *f* of cyt b_6/f; F_0 – minimal fluorescence; F_B or X – iron-sulphur cluster of PSI; F_M – maximal fluorescence; Fd – ferredoxin; FLD – fluorescence decrease; FLI – fluorescence induction; FLR – fluorescence rise; FNR – ferredoxin-$NADP^+$-oxidoreductase; I_{820} – relative transmittance signal measured at 820 nm; MV – 1,1´dimethyl-4,4´-bipyridinium-dichloride (methylviologen); $NADP^+$ and NADPH – oxidised and reduced nicotinamide adenine dinucleotide phosphate; O, K, J, I, P, G, H – particular steps of the FLR; OEC – oxygen evolving complex; P680 or P – electron donor of PSII; P700 or R – electron donor of PSI; PC – plastocyanin; PQ and PQH_2 – oxidised and reduced plastoquinone; PSI – photosystem I; PSII – photosystem II; Q_A or A – first quinone electron acceptor of PSII; Q_B or B - second quinone electron acceptor of PSII; RCII – reaction centre of PSII; RT – room temperature; S_i (i = 0, 1, 2, 3) – redox states of OEC; TM – thylakoid membrane.
Acknowledgements: This work was supported by the Ministry of Education of the Czech Republic by a grant number MSM 6198959215 and through the Marie Curie Initial Training Network of the 7th Framework Programme of the European Union, contract number PITN-GA-2009-238017. The experimental data presented in Fig. 1 are courtesy of Gert Schansker and Petr Ilík.

photosynthetic function (Govindjee 1995). Although FLI technique is popular among researchers, we are still far away from detailed understanding of particular phases of the FLI and of processes hidden behind them (Lazár 1999, 2006). Therefore, further studies of the FLI are needed.

The Chl *a* FLI consists from a fast fluorescence rise (FLR) followed by a slow fluorescence decrease (FLD). The FLR reflects mainly the light-induced photosynthetic reactions, *i.e*., the electron transport in and from photosystem II (PSII) to plastoquinone (PQ) pool, cytochrome (cyt) b_6/f, plastocyanin (PC), photosystem I (PSI), ferredoxin (Fd), and FNR to form reduced nicotinamide adenine dinucleotide phosphate (NADPH). The light-induced electron transport is also associated with accumulation of protons in lumen which are subsequently transported through ATP-synthase to form ATP in stroma. On the other hand, the FLD reflects, in additions to the above, also the dark photosynthetic reactions. Upon illumination of the sample, fluorescence starts to rise from its minimal level (F_0; the O step) to its maximal level (F_M, the P step). A shape of the FLR depends, among others, on the used intensity of excitation light: at room temperature (RT) upon a low light excitation [~ 50–100 μmol(photon) m^{-2} s^{-1}) one step, the I step, appears between the O and P steps and the O-I-P FLR is detected whereas upon a high light excitation [~ 3000 μmol(photon) m^{-2} s^{-1}] two steps, the J and I steps, appear between the O and P steps and the O-J-I-P FLR is measured (Strasser *et al*. 1995, Tomek *et al*. 2001). Typically, the J and I steps appear at about 2 and 30 ms, respectively, and the P step is reached at about 200 ms (Fig. 1). Intactness of the sample is another factor affecting the shape of the O-J-I-P FLR: while well-pronounced J and I steps are detected at RT with leaves and intact chloroplasts, the steps are less pronounced (mainly the I step) when measured at RT with suspension of thylakoid membranes (TM) (Pospíšil and Dau 2002, Joly *et al*. 2005) and the I step disappears when measured with PSII membranes (Pospíšil and Dau 2000, Heredia and De Las Rivas 2003). If the rate of electron transport from P680 (electron donor of PSII) to the PSII acceptor side exceeds the rate of electron transport to P680 from the PSII donor side, *e.g*. in the case of a high-temperature stress of a sample, a new step, the K step, appears at about 300 μs (Guissé *et al*. 1995, Lazár and Ilík 1997, Strasser 1997). Further, some samples (foraminifers, zooxanthellae, lichens and some algae) have P level split into to steps called G and H (Tsimilli-Michael *et al*. 1998, Ilík *et al*. 2006).

It is widely accepted that the variable fluorescence originates only from PSII and that PSI emits only a constant fluorescence (Dau 1994). The basic explanation of the PSII variable fluorescence is that it reflects amount of the so called closed reaction centres of PSII (RCII) that means, in the simplest and very often used approximation, centres with reduced first quinone electron acceptor of PSII, Q_A (Duysens and Sweers 1963). However, effects of the other PSII electron carriers and mechanisms occurring in PSII were also suggested (Lazár 1999, 2006). Moreover, light-induced changes in transmittance signal measured at 820 nm (I_{820} signal), which reflects amount of oxidised P700 (electron donor of PSI) and of oxidised PC (Harbinson and Woodward 1987, Klughammer and Schreiber 1994) revealed that a minimum in I_{820} signal (reflects maximal oxidation of P700 and PC) is reached at the position of the I step of the O-J-I-P FLR (Schansker *et al*. 2003). Further, when electron transport inhibitor 2,5-dibromo-3-methyl-6-isopropyl-p-benzoquinone (DBMIB; inhibits reoxidation of reduced PQ molecules in cyt b_6/f) or electron acceptor 1,1´dimethyl-4,4´-bipyridinium-dichloride (methylviologen (MV); accepts electrons from iron-sulphur cluster of PSI) are applied, the I_{820} signal only decreases and height of the I step increases, almost reaching maximal fluorescence level (DBMIB case), or the I-P phase of the FLR decreases (MV case) (Schansker *et al*. 2005). The above facts indicate that the electron transport reactions occurring beyond PSII also affect the O-J-I-P FLR, mainly the I-P phase.

In addition to experiments, another way to study photosynthesis is to perform theoretical simulations of measured photosynthetic quantities on the basis of known structure, function and kinetics of the photosynthetic system. Although a theoretical approach is generally overlooked, using this approach, it is possible to gain deeper insight into the nature of studied processes, namely to confirm or disprove suggested mechanisms and to resolve and quantify to which extent given mechanism contribute to measured quantity. Further, in silico parameters can be varied that are difficult to change in living sample: by showing how the simulated quantity changes in response to changes in certain parameters can help experimentalists to interpret their measurements more precisely, suggesting which parameters could be important and which could probably be ignored. So far, a mathematical modelling related to plant research was mainly devoted to modelling of plant metabolic biochemical pathways (Giersch 2000, Rios-Estapa and Lange 2007).

The O-J-I-P FLR was theoretically simulated mainly on the basis of models describing, in different complexity, function of PSII and PQ pool only (Lazár *et al*. 1997, Stirbet *et al*. 1998, Vredenberg 2000, Tomek *et al*. 2001, Sušila *et al*. 2004, Zhu *et al*. 2005). However, even using a very detailed model of homogeneous PSII, Lazár (2003) was not able to simulate typical O-J-I-P FLR but only a curve with the J step and with a maximum at the position of the I step (similar to the curve measured after DBMIB-treatment). It implies from the results of Lazár (2003) that PSII model alone is not enough for simulations of typical O-J-I-P FLR that agrees with the above mentioned conclusion based on measurements of the I_{820} signal (Schansker *et al*. 2003, 2005), that is,

electron transport reactions occurring beyond PQ pool also affect the shape of the FLR. Even if simulations of the FLR based on models which included electron transport reactions occurring beyond PQ pool have been published, too (Lebedeva *et al*. 2002, Kroon and Thoms 2006, Laisk *et al*. 2006), the papers did not deal with description of the effect of the reactions on the FLR and they also did not simulate the I_{820} signal paralleling the FLR. For more details on modelling of the Chl *a* FLR *see* recent reviews by Lazár and Schansker (2009), Rubin and Riznichenko (2009) and Vredenberg and Prášil (2009).

In this work a model of electron transport reactions occurring in PSII, PQ pool, cyt b_6/f, PC, PSI, Fd, and FNR is described and used for simulations of both the O-J-I-P FLR and I_{820} signal paralleling the FLR. The model is also successfully used for simulations of the two quantities measured after DMBIB- or MV-treatment and measured upon different intensities of excitation light. Roles of changes of some model parameters on the shape of the simulated quantities are also described and discussed. Results of this work confirm that electron transport reactions occurring behind PQ pool affect the shape of the O-J-I-P FLR and show that theoretical modelling can be useful for better understanding of photosynthetic function.

Description of the model and the used theoretical approach

Detailed description and reaction scheme of the model together with exact definitions of fluorescence and I_{820} signals are given in the Appendix. For the readers who are not interested in theoretical details of the modelling, a more formal but still sufficient description of the model is given below. A sketch of the light photosynthetic reactions occurring in TM and adjacent lumen and stroma spaces between electron carriers considered in the model used here is shown in Scheme 1. The model considers PSII with oxygen eveolving complex (OEC), cyt b_6/f and PSI pigment protein complexes, PQ pool in TM, PC in lumen and Fd and FNR in stroma. A description of the reactions occurring in the model is as follows: absorption of a quantum of light (hν) by PSII causes charge separation leading to formation of oxidised electron donor of PSII, $P680^+$, and Q_A^-. Consequently $P680^+$ is reduced by electrons donated from S_i-states (i = 0, 1, 2, 3) of oxygen evolving complex (OEC) during the S_i-S_{i+1} transitions. The electron stored in Q_A^- is transported to the second quinone electron acceptor of PSII, Q_B, which is two-electron acceptor. When Q_B^{2-} is formed and protonated by two protons from stroma (considered implicitly in the model), it is exchanged with oxidised PQ molecule from the PQ pool forming thus oxidised Q_B again and reduced PQ molecule in the pool. The reduced PQ molecule moves in the membrane to the lumenal side of cyt b_6/f where it donates one electron to haem *f* (through iron-sulphur cluster, Rieske protein, which is considered implicitly) of cyt b_6/f and one electron to low-potential haem *b* (b_L) of cyt b_6/f. The release of the two electrons from reduced PQ molecule is accompanied by a release of two protons to lumen (not considered in the model) leading thus to formation of oxidised PQ molecule. The electron stored in b_L is transported to high-potential haem *b* (b_H) in stromal side of cyt b_6/f. The model also considers existence of haem *c* (*c*), also sometimes denoted as haem *x*, in cyt b_6/f which is assumed to be in a kinetic equilibrium with b_H forming thus two-electron carrier $b_H{\cdots}c$. After two-electron reduction of $b_H{\cdots}c$, the electrons, together with two protons from stroma (considered implicitly in the model), are transported to oxidised PQ molecule from the pool leading to formation of reduced PQ molecule. The electron transport from reduced PQ molecule to cyt b_6/f and back to oxidised PQ molecule as described above is known as the Q-cycle of cyt b_6/f function (Cramer and Zhang 2006). Although also the semi-Q-cycle was described in literature (Joliot and Joliot 1994), for simplicity it is not considered here. The electron stored in haem *f* of cyt b_6/f is transported to oxidised PC molecule which freely moves in lumen and thus reduced PC transports the electron to oxidised electron donor of PSI, $P700^+$. $P700^+$ was formed by a charge separation after absorption of a quantum of light (hυ) by PSI. As all the electron transport reactions occurring in PSI are very fast (Santabarbara *et al*. 2005), only the final electron acceptor in PSI, iron-sulphur cluster F_B, is considered in the model and the charge separation occurring in PSI results in formation of reduced F_B, in addition to formation of $P700^+$. The electron stored in F_B is then transported to Fd, which freely moves in stroma. Electron from Fd is transported to FNR which is assumed to be in stroma too and which is inactive in dark-adapted state and must be activated before the electron transport. When active FNR is doubly reduced, it is converted back to its oxidised active state which reflects formation of NADPH from $NADP^+$, which, however, is not explicitly considered in the model. The reduced Fd can also move to cyt b_6/f where it can donate the electron to $b_H{\cdots}c$ enabling thus Fd-dependent cyclic electron transport (CET) around PSI (Bukhov and Carpentier 2004). Although also Fd-independent CET around PSI was described in literature (Johnson 2005), for simplicity it is not considered here.

A view to Scheme 1 might suggest that the model considered here is rather simple because not all known electron carriers are considered. However, the goal of this work was to formulate a simple model but without loosing quality of simulated curves. Further, the impression of simplicity of the model is only apparent and when the model is written by means of its all particular reactions, rather complicated reaction scheme is obtained (*see* Appendix).

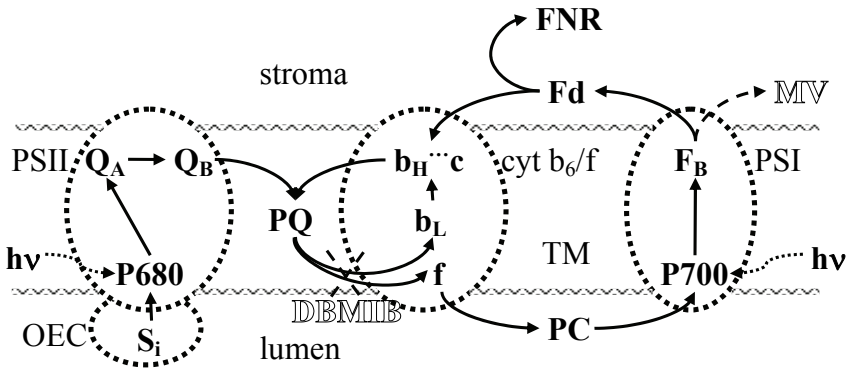

Scheme 1. A sketch of the light photosynthetic reactions occurring in TM, and adjacent lumen and stroma spaces, between electron carriers considered in the model. Action of DBMIB and MV is also shown. *See* Appendix for more details.

Input parameters of the model are relative initial amounts (for dark-adapted state) of particular electron carriers and values of rate constants of particular reactions. The values of the input parameters are listed in the Appendix where also exact definitions of fluorescence and I_{820} signals are given. Shortly mentioned here, fluorescence signal was assumed to be proportional to the amount of Q_A^-, considering also the energetic connectivity of PSIIs and fluorescence quenching by oxidised PQ molecules and I_{820} signal was assumed to be proportional to the amount of oxidised P700 and oxidised PC, considering molar extinction coefficients of the two components.

In the study presented here, simulations of the FLR and I_{820} signal are performed for given values of the input parameters. The simulations are preferred over fitting of the model parameters to obtain the best agreement between theory and experiments because in a complex system (as presented here) a change in value of one model parameter can be compensated by a change in value of another model parameter without loosing quality of the fit (Baake and Schlöder 1992). Moreover, even if the best fit is found, the obtained values of parameters need not agree with values known from the literature (Strasser and Stirbet 2001) and the researcher has to judge if the obtained results are really meaningful. The simulations were performed using free software *GEPASI version 3.21* (*P. Mendes*, The University of Wales, Aberystwyth, UK) that was designed for the simulation of chemical and biochemical kinetics (Mendes 1993). With respect to the simulations presented here, it is important to keep in mind that already a qualitative agreement between experiment and theory is a useful result in the case of modelling of the FLR and I_{820} signal because the two quantities are manifestations of a very complex biological system and therefore hard to describe correctly and comprehensively. This is quite different from modelling of technical systems that can be described correctly and where a quantitative agreement between experiments and theory is strictly required.

Results and discussion

Experimental data: To verify any theoretical model, its theoretical simulations must be compared with suitable experimental data. In this work not only the O-J-I-P FLR and I_{820} signal measured with the control (no treatment) sample are used to verify the model but further experimental data are used, enabling thus much better verification and validation of the model and consequently the processes described by the model. Fig. 1 shows experimental FLRs (Fig. 1*A,C*) and I_{820} signals (Fig. 1*B,D*) measured at RT with control (no treatment), DBMIB- and MV-treated samples (Fig. 1*A,B*) and measured at RT with control samples upon different intensities of excitation light (Fig. 1*C,D*). For the control sample, position of the minimum in the I_{820} signal (Fig. 1*B*) agrees with position of the I step in the FLR (Fig. 1*A*). DBMIB-treatment causes an increase of the I step (Fig. 1*A*) which almost reaches maximal fluorescence level and the I_{820} signal only decreases (Fig. 1*B*). In the case of MV-treatment, the I-P phase of the FLR is not so pronounced (Fig. 1*A*) and the I_{820} signal also only decreases but at the end of the measurement the I_{820} signal is higher than the I_{820} signal of DBMIB-treated sample (Fig. 1*B*). The decrease in the intensity of excitation light used for the measurements leads to disappearance of the J step, to a decrease of the relative height of the I step and to a shift of its position to longer times, and to a shift of the P step to longer times as well (Fig. 1*C*). Relative deepness of the minimum of the I_{820} signal is reduced and positions of the minima are a little bit shifted to longer times upon decreasing of the intensity of excitation light (Fig. 1*D*).

Simulations for the control, DBMIB- and MV-treated samples: Fig. 2 shows simulations of the FLRs (Fig. 2*A*) and I_{820} signals (Fig. 2*B*) for the control, DBMIB- and MV-treated samples. Generally, when the theoretical simulations shown in Fig. 2 are compared with related experimental data (Fig. 1*A,B*), a very good qualitative agreement is found. The simulated FLR of the control shows the J, I and P steps at positions very similar to the experimental FLR. However, the J and I steps in the simulated FLR are not so pronounced and resemble the

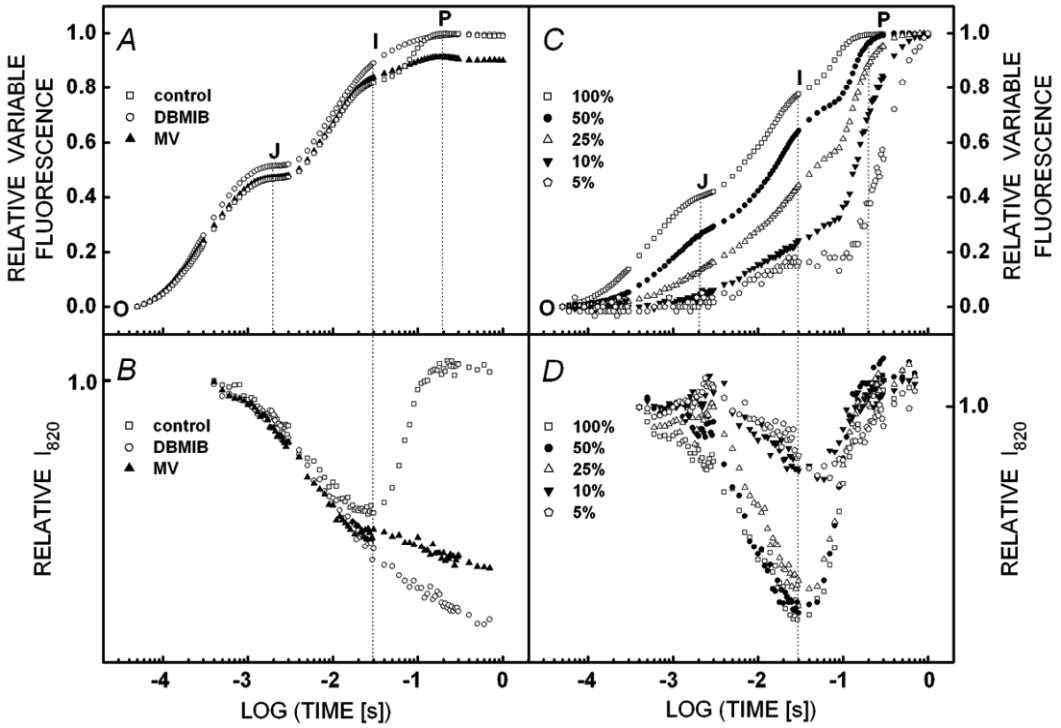

Fig. 1. Experimental FLRs (*A,C*) and I_{820} signals (*B,D*) measured at RT with control (no treatment), DBMIB- and MV-treated samples (*A,B*) and measured at RT with control samples upon different intensities of excitation light (*C,D*). The FLRs are presented by means of relative variable fluorescence [= $(F(t) - F_0)/(F_M - F_0)$] where F_M of control sample was used for the case of DBMIB- and MV-treated samples. Particular steps of the FLR are denoted. The I_{820} signals at 400 μs are normalized to 1. The FLR and related I_{820} signal were measured simultaneously using a dual channel *Plant Efficiency Analyser* (*Hansatech Instruments*, King's Lynn, Norfolk, UK) and intensity of excitation red (650 nm) light of 3000 μmol m^{-2} s^{-1} (*A,B*) and 100 *%* in panels *C,D* corresponding to 1800 μmol(photon) m^{-2} s^{-1}. All data were measured with dark-adapted pea leaves. The data are from Schansker *et al*. (2005) (*A,B*) and Ilík *et al*. (2006) (*C,D*) where more details of the measurements can be found.

FLR measured with TMs (Pospíšil and Dau 2002, Joly *et al*. 2005). The reason of not so pronounced J and I step might be that no functional heterogeneities of the pigment-protein complexes and electron carriers were assumed in the model presented here (*see* Appendix). Time courses of model forms which contribute to the simulated FLR (model forms with reduced Q_A; *see* Appendix) are for simulation of the FLR of the control shown in Fig. 3*A* and agree generally with the time courses obtained in other studies (Stirbet *et al*. 1998, Tomek *et al*. 2001, Zhu *et al*. 2005). The I_{820} signal simulated for the control shows the same qualitative behaviour as the experimental signal, *i.e*., a minimum of the I_{820} signal (reflecting maximal accumulation of oxidised P700 and PC) appears approximately at the position of the I step of the FLR. As the I_{820} signal has never been simulated before, more attention is paid to its explanation. While oxidised P700 starts to accumulate sooner than oxidised PC (Fig. 3*B*, left y-axis), maximal accumulation of oxidised P700 is about a half of that of oxidised PC. But because the molar extinction coefficient of oxidised P700 is more than six times higher than that of oxidised PC (*see* Appendix), the maximal I_{820} signal (*i.e*., its minimum) caused by oxidised P700 is about three times higher than that of oxidised PC (Fig. 3*B*, right y-axis). When contributions to overall I_{820} signal in its minimum (17 ms) caused by oxidised P700 and oxidised PC is quantified from related curves in Figs. 2*B*, 3*B*, oxidised P700 and oxidised PC contribute by 75% and 25%, respectively. These values are a little bit different from results of Schansker *et al*. (2003) who found that ratio between contributions of oxidised PC to oxidised P700 is 50/50 and 40/60 for pea and *Camellia* leaves, respectively, but agree more with the ratio found in other studies (*see* Schansker *et al*. 2003 and references therein). However note that separation of overall I_{820} signal into two independent I_{820} signals is not fully justified (*see* Appendix) and therefore the here-evaluated contributions mentioned above must be understood as estimates.

The FLRs (Fig. 2*A*) and I_{820} signals (Fig. 2*B*) simulated for the DBMIB- and MV-treated samples show the same qualitative changes as in the experimental curves (Fig. 1*A,B*), *i.e*., the height of the I step increases reaching maximal fluorescence level (DBMIB case) and the I-P phase of the FLR is not so pronounced (MV case). These simulations clearly show an effect of the electron transport reactions occurring beyond PSII on the shape of the FLR. Different time courses of $P680Q_A^-Q_B^{2-}$ model

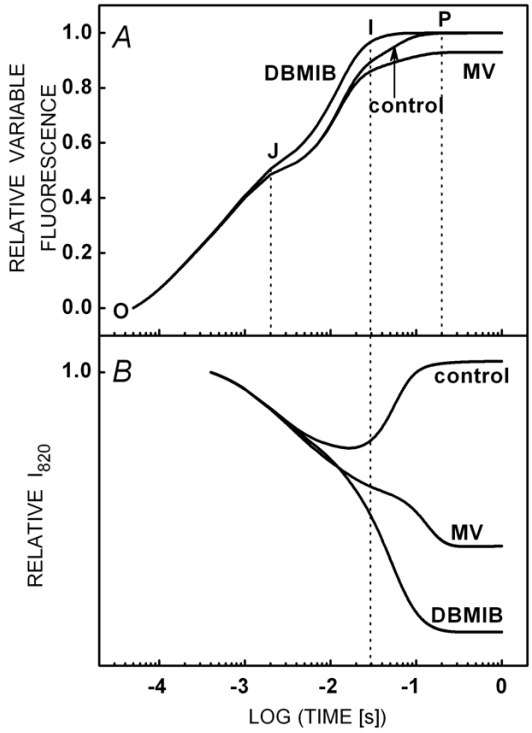

Fig. 2. Simulated FLRs (*A*) and I_{820} signals (*B*) for control (no treatment), DBMIB- and MV-treated samples. The FLRs and I_{820} signals are presented in the same way as in Fig. 1.

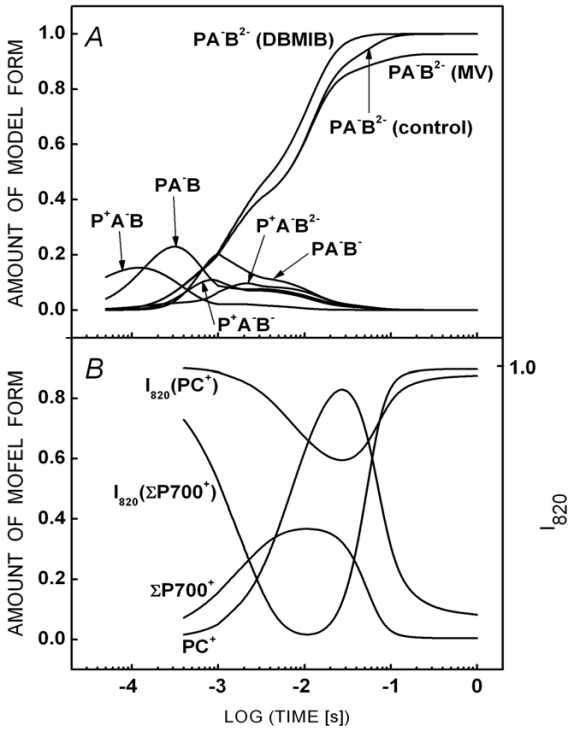

Fig. 3. Time courses of model forms that contribute to the FLR simulated for the control sample (*A*) and time courses of PC^+ and sum of $P700^+$ (left y-axis) and their contributions to the I_{820} signal (right y-axis) simulated for the control sample (*B*). P, A and B in panel *A* mean P680, Q_A and Q_B, respectively (*see* Appendix). Panel *A* also shows time courses of the PA^-B^{2-} model form simulated for the DBMIB- and MV-treated samples.

forms (Fig. 3*A*) are the main reason of the changes in the FLRs simulated for the DBMIB- and MV-treated samples whereas time course of the other model forms simulated for the DBMIB- and MV-treated samples are very similar to those of the control sample (data not shown). In agreement with the experiments (Fig. 1*B*), final value of the I_{820} signal simulated for the DBMIB-treated sample reaches significantly lower value than the I_{820} signal simulated for the MV-treated sample (Fig. 2*B*). Such behaviour is caused by the fact that DBMIB blocks reoxidation of reduced PQ molecules in cyt b_6/f (Schansker *et al*. 2005 and references therein) leading to no possibility to re-reduce oxidised PC, which reaches its maximal possible oxidation at about 190 ms (Fig. 4*A*, left y-axis). The lack of electrons supplied to PC also causes oxidation of P700, which reaches its maximal possible value at about 345 ms (Fig. 4*A*, left y-axis). On the other hand, as MV accepts electrons from iron-sulphur cluster of PSI (Schansker *et al*. 2005 and references therein), the MV-treatment causes an additional electron flux from PSI, when compared to the control sample, enabling thus more charge separations in PSI and hence more significant accumulation of oxidised P700 and consequently of oxidised PC (Fig. 4*B*, left y-axis) when compared to the control sample (Fig. 3*B*, left y-axis). However, maximal accumulation of oxidised P700 and of oxidised PC for the MV-treated sample is not as high as in the case of the DBMIB-treated sample (Fig. 4*A,B*; left y-axes). Further, the same as in the case of the simulations performed for the control sample (Fig. 3*B*), even if more oxidised PC accumulates than oxidised P700 for both the DBMIB- and MV-treated samples (Fig. 4*A,B*; left y-axes) because the molar extinction coefficient of oxidised P700 being more than six times higher than that of oxidised PC (*see* Appendix), the contribution of oxidised P700 to the I_{820} signal is much higher than the contribution of oxidised PC to the I_{820} signal (Fig. 4*A,B*; right y-axes).

Simulations for different intensities of excitation light: Fig. 5 shows simulations of the FLRs (Fig. 5*A*) and I_{820} signals (Fig. 5*B*) for different intensities of excitation light. Generally, the same as in the case of the simulations performed for the DBMIB- and MV-treated samples (*see* above), when the theoretical simulations shown in Fig. 5 are compared with related experimental data (Fig. 1*C,D*), a good qualitative agreement is found. However, disappearance of the J step and decrease of the relative height of the I step as observed in the experiments upon decreasing intensity of excitation light (Fig. 1*C*) is not so straightforward in the simulations (Fig. 5*A*). Instead, the J step seems to decrease its relative height and to shift its position to longer times whereas the

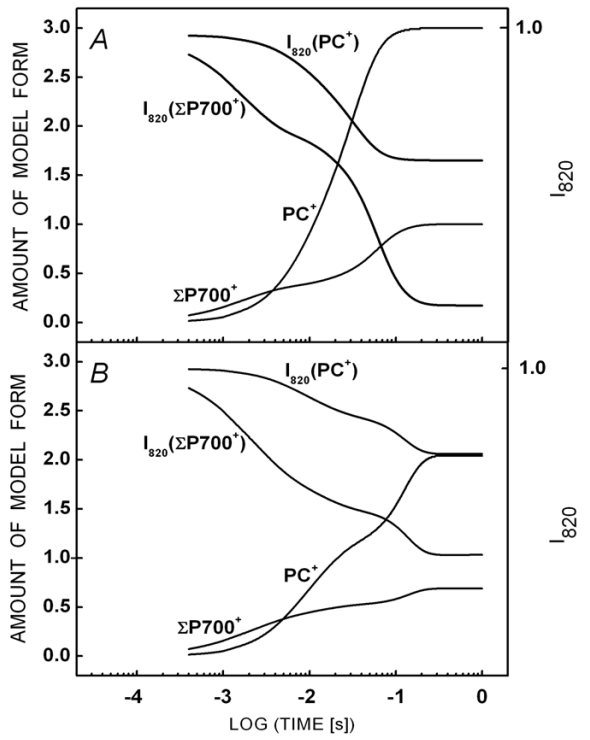

Fig. 4. Time courses of PC^+ and sum of $P700^+$ (left y-axes) and their contributions to the I_{820} signal (right y-axes) simulated for the DBMIB- (*A*) and MV-treated (*B*) samples. For better comparison of changes in the time courses, the left y-axes as well as the right y-axes have the same scale in both panels.

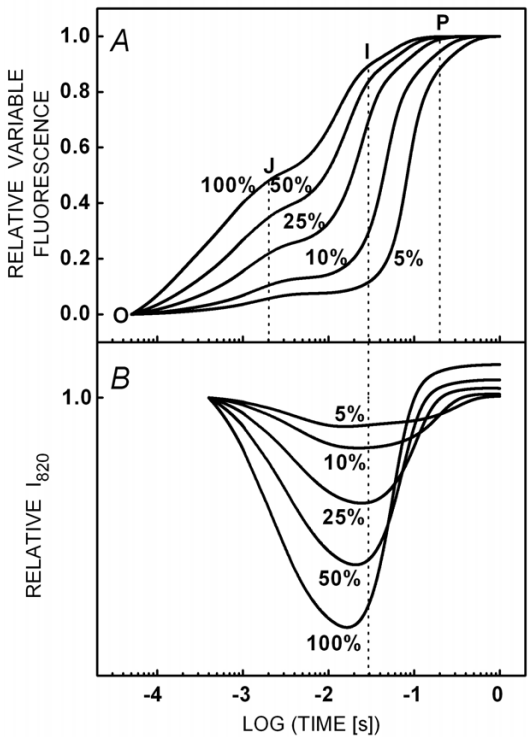

Fig. 5. Simulated FLRs (panel A) and I_{820} signals (panel B) for different intensities of excitation light. The FLRs and I_{820} signals are presented in the same way as in Fig. 1.

I step seems to disappear upon the decrease of the intensity of excitation light. The reason for such behaviour might be again the fact that no functional heterogeneities of the pigment-protein complexes and electron carriers were assumed in the model presented here. However, upon decreasing of the intensity of excitation light position of the P step is shifted to longer times in the simulations (Fig. 5*A*) in agreement with the experiments (Fig. 1*C*). The changes in the shapes of the O-J-I phase of the FLRs simulated for decreasing intensity of excitation light are caused by a decrease of transient maximal accumulations of all the model forms responsible for fluorescence signal except of $P680^+Q_A^-Q_B^{2-}$ model form (data not shown). Although the latter model form decreases its transient accumulation in the O-J-I phase of the FLRs upon decreasing intensity of excitation light, it always reaches its maximal value in the position of the P step and is responsible for the I-P phase of the FLR (data not shown). Generally, the changes in time courses of the model forms responsible for the FLRs simulated for different intensities of excitation light are in agreement with previous studies (Tomek *et al*. 2001).

The changes in the I_{820} signal simulated for different intensities of excitation light (Fig. 5*B*) show the same behaviour as the experimentally measured changes (Fig. 1*D*), *i.e.*, a reduction of deepness of the minimum of I_{820} signal and its shift to longer times upon decreasing intensity of excitation light. The origin of the reduction of the deepness of the minimum of I_{820} signal is that a lower intensity of excitation light causes less charge separations in PSI and hence less accumulation of oxidised P700 and consequently of oxidised PC when compared to a higher intensity of excitation light. As for time courses of oxidised P700 and oxidised PC (positions and extents of transient maximal accumulations) and their contributions to the I_{820} signal, the same holds (data not shown) as mentioned above for simulation of the I_{820} signal of the control (*i.e.*, 100% intensity of excitation light) sample.

Further in silico experiments: Theoretical simulations presented above showed a robustness of the model introduced here, *i.e.*, the model is able to qualitatively simulate changes in light-induced fluorescence and I_{820} signals caused by different chemical treatments and by different intensities of excitation light in agreement with experimental data. Below are presented some further in silico experiments; mainly those ones which test suggestions made elsewhere on the basis of the FLR and I_{820} signal measurements.

It is usually assumed in the simulations of the FLR that the PQ pool is initially fully oxidised (*e.g.*, Lazár 2003). On the other hand, Feild *et al*. (1998) measured an increase of F_0 in dark, after previous illumination of sunflower leaves, which they interpreted to be due to a nonphotochemical reduction of PQ pool caused by chlororespiration pathway as originally found by

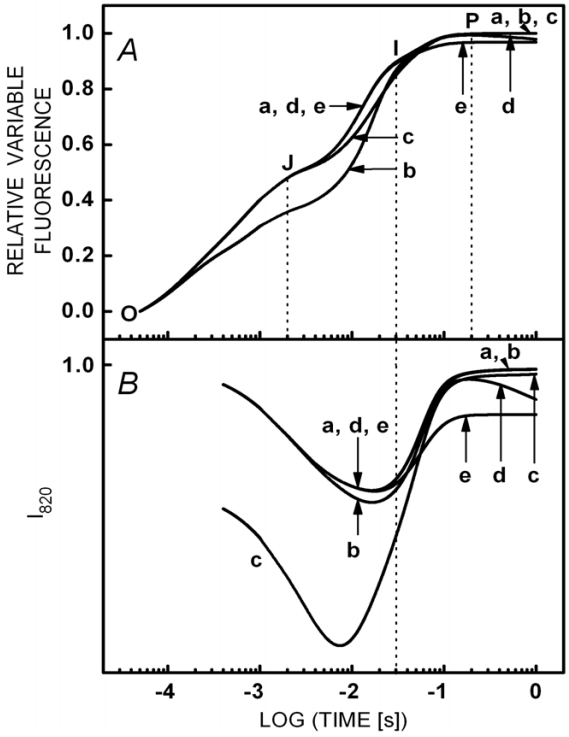

Fig. 6. Simulated FLRs (*A*) and I_{820} signals (*B*) for different values of selected model parameters. For better presentation, the FLRs are presented by means of the relative variable fluorescence where F_M of the control sample was used for the normalization (*see* Fig. 1). Curves a – control (no treatment) sample, curves b – PQ pool is initially fully oxidised, curves c – PC is initially fully oxidised, curves d and e – rate constant of FNR activation is 1 and 100 s^{-1}, respectively.

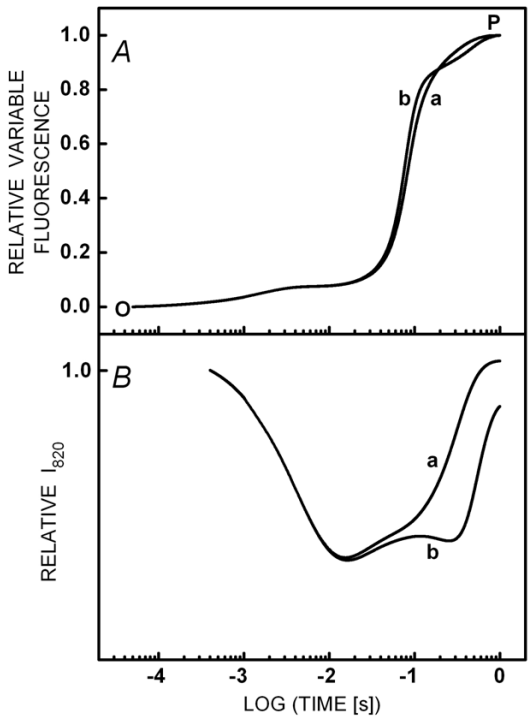

Fig. 7. FLRs (*A*) and I_{820} signals (*B*) simulated for a low intensity of excitation light (5 %) with (curves a) and without (curves b) consideration of the CET around PSI in the model. The FLRs and I_{820} signals are presented in the same way as in Fig. 1.

Bennoun (1982). This fact suggests that the PQ pool might not be completely oxidised in dark. Therefore, it was assumed in all previous simulations, that the PQ pool is initially by half oxidised and by half reduced. To explore the effect of the initial redox state of the PQ pool on the FLR and I_{820} signal, simulations of the quantities were performed also for initially completely oxidised PQ pool (Fig. 6, curves b). When compared with the control curves (PQ is initially by half oxidised and by half reduced; Fig. 6, curves a), the initial oxidation of PQ pool results mainly in the lowering of the J step in the FLR which consequently causes not so pronounced the I step (Fig. 6*A*, curve b). These results are in agreement with literature (Stirbet *et al*. 1998). The initially oxidised PQ pool causes more oxidised PC and P700 during illumination, that results in a more pronounced minimum of the I_{820} signal (Fig. 6*B*, curve b) when compared with the I_{820} signal obtained for the partial initial reduction of the PQ pool (Fig. 6*B*, curve a). As the shape of the FLR simulated for the partial initial reduction of the PQ pool better agrees with experimental FLR than the FLR simulated for initially fully oxidised PQ pool, the pool seems to be really reduced to some extent in dark.

Based on measurements of the FLR and I_{820} signal, Schansker *et al*. (2003) concluded that PC must be reduced in the dark-adapted state. Fully reduced PC was assumed also in all previous simulations (*see* Appendix) and with this assumption typical O-J-I-P FLR and I_{820} signal were simulated. To test if the assumption of initially reduced PC is important for correct simulations of the FLR and I_{820} signal, the simulations were performed also for the case of PC being initially fully oxidised (Fig. 6, curves c). The results show that initial oxidation of PC causes disappearance of the I step in the FLR and the initial I_{820} signal at 400 μs is much lower (in agreement with initially oxidised PC) than when compared with the I_{820} signal of the control sample (Fig. 6, curves a). If normalization of the simulated I_{820} signal at 400 μs to 1 was used (as in the experiments, *see* Fig. 1), the signal would significantly rise above unity at the end of simulation (data not shown). Hence, the shapes of the FLR and I_{820} signal, which are not in agreement with experimental data, clearly demonstrate that PC must be initially reduced.

Analysis of experimental FLR and I_{820} signal data measured with higher plants led to suggestion that FNR is initially inactive and slowly activates during illumination of the sample (Schansker *et al*. 2003, 2005) in agreement with previous literature (Carrillo *et al*. 1981, Satoh 1981). Further, a decrease of fluorescence signal appearing after reaching a fluorescence maximum at about 200 ms in some organisms (foraminifers, zooxanthellae, lichens, and

some algae; *see*, *e.g.*, Tsimilli-Michael *et al*. 1998, Ilík *et al*. 2006), and paralleled by a decrease in I_{820} signal, was suggested (Ilík *et al*. 2006) to be caused by an increased rate (when compared with the higher plants) of FNR activation. In all previous simulations, the value of the rate constant of FNR activation was set to 0.01 s^{-1} (*see* Appendix). To test the previous suggestions on activation of FNR, in silico experiments were performed for increased value of the rate constant of FNR activation. When the value of the rate constant of FNR activation was set to 1 s^{-1}, fluorescence as well as the I_{820} signals decreased (Fig. 6, curves d) after reaching their maximal values at about 200 ms, in agreement with the experimental findings mentioned above. However, when the rate constant of FNR activation was further increased and set to 100 s^{-1}, the I-P phase of the FLR as well as the I_{820} signal at the end of the simulation were diminished (Fig. 6, curves e) which is not in agreement with the above mentioned experimental data. Therefore, in agreement with the above mentioned suggestions based on experimental results, to obtain typical O-J-I-P FLR and I_{820} signal as measured with higher plants, a slow activation of FNR is necessary, and the rate of the activation must be increased (but not too much) to obtain a decrease of fluorescence and I_{820} signal after about 200 ms as observed in some organisms.

As the CET around PSI mainly occurs in the induction period (Holtgrefe *et al*. 2003, Joliot and Joliot 2005), *i.e*., also during the FLR, the CET is also included in the model introduced here (*see* Schemes 1 and A1). The following in silico experiments explored if the CET around PSI really must be considered in the model to successfully simulate the FLR and I_{820} signal. The FLRs simulated for the control sample (*i.e*., 100% intensity of excitation light) with or without consideration of the CET are almost identical and there is only a minor change in the I_{820} signals (a little bit deeper minimum for the case of omitted CET; data not shown). Hence, the CET around PSI has a minor role for the shape of the FLR and I_{820} signal upon high intensity of excitation light. However, the changes in the FLR and I_{820} signal with or without considered CET are more pronounced in the simulations performed for a low intensity of excitation light (5%; Fig. 7*A,B*). A smooth increase of fluorescence signal starting from about 10 ms for the case when the CET is considered in the model (Fig. 7*A*, curve a) is changed into a two-phase increase when the CET is not considered (Fig. 7*A*, curve b). Also the time course of the I_{820} signal is more complex and does not rise to the starting value at the end of simulation for the case when the CET is not considered (Fig. 7*B*, curve b). Taking together, both the FLR and I_{820} signal simulated for a low intensity of excitation light without consideration of the CET around PSI do not agree with experimental data (Fig. 1*C,D*). Therefore, the CET around PSI seems to play a role for the shape of the FLR and I_{820} signal in the case of a low intensity of excitation light and thus, generally, the CET must be considered in the model. The necessity of CET revealed from the simulations only for the case of a low intensity of excitation light is in agreement with the above mentioned occurrence of CET mainly in the induction period where the induction period must be understood as a period when the electron transport chain is not fully reduced. This state of the electron transport chain is more easily obtained for a low intensity of excitation light than for a high intensity of excitation light where the electron transport chain is immediately fully reduced and consequently the effect of CET is not revealed from the simulations.

Relation to other models: Successful simulations of the FLRs and I_{820} signals as measured upon different experimental conditions and also the other in silico experiments demonstrate robustness of the model presented here. So far, most of the models used for simulations of the FLR were based on description of electron transport reactions occurring in PSII and PQ pool only (*e.g*., Lazár *et al*. 1997, Stirbet *et al*. 1998, Vredenberg 2000, Tomek *et al*. 2001, Sušila *et al*. 2004, Zhu *et al*. 2005). More or less, authors of the models claimed that the models are able to successfully simulate the FLR. Consideration of only the PSII and PQ pool reactions in the models is caused by the fact that PSII is generally assumed to be the only source of variable fluorescence (*see* Introduction): hence, why to consider electron transport reactions occurring beyond PSII and PQ pool? However, in the light of previous experimental findings (Schansker *et al*. 2003, 2005) and the results presented here, *i.e*., the electron transport reactions occurring beyond PSII and PQ pool play a significant role for the shape of the FLR, a restriction of a model for the FLR only to electron transport reactions occurring in PSII and PQ pool, as an application of the Occam's razor rule, seems to be an oversimplification and might be misguided for correct interpretation of the FLR.

Only three models published so far considered also the electron transport reactions occurring beyond PSII and PQ pool (Lebedeva *et al*. 2002, Kroon and Thoms 2006, Laisk *et al*. 2006). However, no analysis on necessity of these reactions for the modelling of the FLR was performed. In the model presented here, the necessity of these reactions also implies from simulations of the I_{820} signal which reflects redox states of P700 and PC. The three papers mentioned above also did not simulate the I_{820} signal paralleling the FLR.

Although the model presented here successfully simulated the FLR and I_{820} signal as measured upon different experimental conditions, the agreements between simulations and experimental curves are still "only" qualitative and some discrepancies can be found. As mentioned above, consideration of heterogeneities in function of pigment-protein complexes and electron carriers would probably lead to a quantitative agreement. Moreover, some processes which were not considered in

the model presented here might also play a role, namely formation of light-induced electric potential difference across TM (Schreiber and Neubauer 1990, Dau *et al*. 1991, Pospíšil and Dau 2002, Lebedeva *et al*. 2002, Vredenberg and Bulychev 2002). However, in the author's opinion, the heterogeneities and the other processes would only fine tune the simulated FLR and I_{820} signal whereas one of the goals of this paper was to test whether at all a simple model can (qualitatively) simulate the FLR and the I_{820} signal together.

Conclusion: In the present work the model was used for exploring the function of PSII (*via* FLR) and PSI and PC (*via* I_{820} signal). The model was able to simulate the FLR and I_{820} signal as measured upon different experimental conditions indicating robustness of the model and the fact that the electron transport reactions occurring beyond PSII and PQ pool also affect the shape of the FLR. Besides an improvement of the model (*e.g*., to include the heterogeneities and the processes mentioned above), a potential future application of the model is that it can be used for studying function of the other pigment-protein complex, cyt b_6/f. As cyt b_6/f connects PSII with PSI, correct description of cyt b_6/f function might be crucial for understanding the electron transport in TM. In the present model, the function of cyt b_6/f was described, in addition to internal electron transport and reduction of PC, by the Q-cycle and Fd-dependent CET around PSI. But the model can be easily modified to include also the semi-Q-cycle and Fd-independent CET around PSI. Using the modified model, roles of all the cycles in the electron transport in TM could be studied.

References

Baake, E., Schlöder, J.P.: Modelling the fast fluorescence rise of photosynthesis. – Bull. Math. Biol. **54**: 999-1021, 1992.

Bennoun, P.: Evidence for a respiratory chain in the chloroplast. – Proc. Natl. Acad. Sci. USA **79**: 4352-4356, 1982.

Bukhov, N., Carpentier, R.: Alternative photosystem I-driven electron transport routes: mechanisms and functions. – Photosynth. Res. **82**: 17-33, 2004.

Carrillo, N., Lucero, H.A., Vallejos, R.H.: Light modulation of chloroplast membrane-bound ferredoxin-NADP+ oxido-reductase. – J. Biol. Chem. **256**: 1058-1059, 1981.

Cramer, W.A., Zhang, H.: Consequences of the structure of the cytochrome b_6f complex for its charge transfer pathways. – Biochim. Biophys. Acta **1757**: 339-345, 2006.

Crofts, A.R., Wraight, C.A.: The electrochemical domain of photosynthesis. – Biochim. Biophys. Acta **726**: 149-185, 1983.

Dau, H.: Molecular mechanism and quantitative models of variable photosystem II fluorescence. – Photochem. Photobiol. **60**: 1-23, 1994.

Dau, H., Windecker, R., Hansen, U.-P.: Effect of light-induced changes in thylakoid voltage on chlorophyll fluorescence of *Aegopodium podagraria* leaves. – Biochim. Biophys. Acta **1057**: 337-345, 1991.

Duysens, L.N.M., Sweers, H.E.: Mechanism of the two photochemical reactions in algae as studied by means of fluorescence. – In: Japanese Society of Plant Physiologists (ed.): Studies on Microalgae and Photosynthetic Bacteria. Pp 353-372. Univ.Tokyo Press, Tokyo 1963.

Feild, T.S., Nedbal, L., Ort, D.R.: Nonphotochemical reduction of the plastoquinone pool in sunflower leaves originates from chlororespiration. – Plant Physiol. **116**: 1209-1218, 1998.

Giersch, C.: Mathematical modelling of metabolism. – Curr. Opin. Plant Biol. **3**: 249-253, 2000.

Govindjee: 63 years since Kautsky - chlorophyll *a* fluorescence. – Aust. J. Plant Physiol. **22**: 131-160, 1995.

Guissé, B., Srivastava, A., Strasser, R.J.: The polyphasic rice of the chlorophyll *a* fluorescence (O-K-J-I-P) in heat-stressed leaves. – Arch. Sci. **48**: 147-160, 1995.

Harbinson, J., Woodward, F.I.: The use of light-induced absorbance changes at 820 nm to monitor the oxidation state of P-700 in leaves. – Plant Cell Environ. **10**: 131-140, 1987.

Heredia, P., De Las Rivas, J.: Fluorescence induction of Photosystem II membranes shows the steps till reduction and protonation of the quinone pool. – J. Plant Physiol. **160**: 1499-1506, 2003.

Holtgrefe, S., Bader, K.P., Horton, P., Scheibe, R., von Schaewen, A., Backhausen, J.E.: Decreased content of leaf ferredoxin changes electron distribution and limits photosynthesis in transgenic potato plants. – Plant Physiol. **133**: 1768-1778, 2003.

Ilík, P., Kouřil, R., Fiala, J., Nauš, J., Vácha, F.: Spectral characterization of chlorophyll fluorescence in barley leaves during linear heating. Analysis of high-temperature fluorescence rise around 60°C. – J. Photochem. Photobiol. **59**: 103-114, 2000.

Ilík, P., Schansker, G., Kotabová, E., Váczi, P., Strasser, R.J., Barták, M.: A dip in the chlorophyll fluorescence induction at 0.2 - 2 s in *Trebouxia*-possessing lichens reflects a fast reoxidation of photosystem I. A comparison with higher plants. – Biochim. Biophys. Acta **1757**: 12-20, 2006.

Jablonsky, J., Lazar, D.: Evidence for intermediate S-states as initial phase in the process of oxygen-evolving complex oxidation. – Biophys. J. **94**: 2725-2736, 2008.

Jablonsky, J., Susila, P., Lazar, D.: Impact of dimeric organization of enzyme on its function: the case of photosynthetic water splitting. – Bioinformatics **24**: 2755-2759, 2008.

Johnson, G.N.: Cyclic electron transport in C_3 plants: fact or artefact? – J. Exp. Bot. **56**: 407-416, 2005.

Joliot, A., Joliot, P.: Étude cinétique de la réaction photochimique libérant l' oxygène au cours de la photosynthèse. – C. R. Acad. Sci. **258**: 4622-4625, 1964.

Joliot, P., Joliot, A.: Mechanism of electron transfer in the cytochrome b/f complex of algae: Evidence for a semiquinone cycle. – Proc. Natl. Acad. Sci. USA **91**: 1034-1038, 1994.

Joliot, P., Joliot, A.: Quantification of cyclic and linear flows in plants. – Proc. Natl. Acad. Sci. USA **102**: 4913-4918, 2005.

Joly, D., Bigras, C., Harnois, J., Govindachary, S., Carpentier, R.: Kinetic analyses of the OJIP chlorophyll fluorescence rise in thylakoid membranes. – Photosynth. Res. **84**: 107-112, 2005.

Kirchhoff, H., Schöttler, M.A., Maurer, J., Weis E.: Plastocyanin redox kinetics in spinach chloroplasts: evidence for disequilibrium in the high potential chain. – Biochim.

Biophys. Acta **1659**: 63-72, 2004.

Klughammer, C., Schreiber, U.: An improved method, using saturating light pulses, for the determination of photosystem I quantum yield via $P700^+$-absorbance changes at 830 nm. – Planta **192**: 261-268, 1994.

Kroon, B.M.A., Thoms, S.: From electron to biomass: A mechanistic model to describe phytoplankton photosynthesis and steady-state growth rates. – J. Phycol. **42**: 593-609, 2006.

Kurreck, J., Schödel, R., Renger, G.: Investigation of the plastoquinone pool size and fluorescence quenching in thylakoid membranes and Photosystem II (PS II) membrane fragments. – Photosynth. Res. **63**: 171-182, 2000.

Laisk, A., Eichelmann, H., Oja, V.: C_3 photosynthesis *in silico*. – Photosynth. Res. **90**: 45-66, 2006.

Lazár, D.: Chlorophyll *a* fluorescence induction. – Biochim. Biophys. Acta **1412**: 1-28, 1999.

Lazár, D.: Chlorophyll *a* fluorescence rise induced by high light illumination of dark-adapted plant tissue studied by means of a model of photosystem II and considering photosystem II heterogeneity. – J. Theor. Biol. **220**: 469-503, 2003.

Lazár, D.: The polyphasic chlorophyll *a* fluorescence rise measured under high intensity of exciting light. – Funct. Plant Biol. **33**: 9-30, 2006.

Lazár, D., Ilík, P.: High-temperature induced chlorophyll fluorescence changes in barley leaves - Comparison of the critical temperatures determined from fluorescence induction and from fluorescence temperature curve. – Plant Sci. **124**: 159-164, 1997.

Lazár, D., Jablonský, J.: On the approaches applied in formulation of a kinetic model of photosystem II: Different approaches lead to different simulations of the chlorophyll *a* fluorescence transients. – J. Theor. Biol. **257**: 260-269, 2009.

Lazár, D., Kaňa, R., Klinkovský, T., Nauš, J.: Experimental and theoretical study on high temperature induced changes in chlorophyll *a* fluorescence oscillations in barley leaves upon 2 % CO_2. – Photosynthetica **43**: 13-27, 2005.

Lazár, D., Nauš, J., Matoušková, M., Flašarová, M.: Mathematical modeling of changes in chlorophyll fluorescence induction caused by herbicides. – Pestic. Biochem. Physiol. **57**: 200-210, 1997.

Lazár, D., Pospíšil, P.: Mathematical simulation of chlorophyll *a* fluorescence rise measured with 3-(3´,4´-dichlorophenyl)-1,1-dimethylurea-treated barley leaves at room and high temperatures. – Eur. Biophys. J. **28**: 468-477, 1999.

Lazár, D., Schansker, G.: Models of chlorophyll *a* fluorescence transients. – In: Laisk, A., Nedbal, L., Govindjee (ed.): Photosynthesis *in silico*: Understanding Complexity from Molecules to Ecosystems. Pp 85-123. Springer, Dordrecht 2009.

Lebedeva, G.V., Belyaeva, N.E., Demin, O.V., Riznichenko, G.Y., Rubin, A.B.: A kinetic model of primary photosynthetic processes. Description of the fast phase of chlorophyll fluorescence induction under different light intensities. – Biofizika **47**: 1044-1058, 2002.

McClendon, J.H., Fukshansky, L.: On the interpretation of absorption-spectra of leaves. 2. The nonabsorbed ray of the sieve effect and the mean optical pathlength in the remainder of the leaf. – Photochem. Photobiol. **51**: 211-216, 1990.

Mendes, P.: GEPASI - a software package for modelling the dynamics, steady states and control of biochemical and other systems. – Comput. Appl. Biosci. **9**: 563-571, 1993.

Oja, V., Bichele, I., Hüve, K., Rasulov, B., Laisk, A.: Reductive titration of photosystem I and differential extinction coefficient of $P700^+$ at 810–950 nm in leaves. – Biochim. Biophys. Acta **1658**: 225-234, 2004.

Pospíšil, P., Dau, H.: Chlorophyll fluorescence transients of Photosystem II membrane particles as a tool for studying photosynthetic oxygen evolution. – Photosynth. Res. **65**: 41-52, 2000.

Pospíšil, P., Dau, H.: Valinomycin sensitivity proves that light-induced thylakoid voltages result in millisecond phase of chlorophyll fluorescence transients. – Biochim. Biophys. Acta **1554**: 94-100, 2002.

Rios-Estepa, R., Lange, B.M.: Experimental and mathematical approaches to modeling plant metabolic network. – Phytochemistry **68**: 2351-2374, 2007.

Rubin, A.B., Riznichenko, G.: Modeling of the primary processes in a photosynthetic membrane. – In: Laisk, A., Nedbal, L., Govindjee (ed.): Photosynthesis *in silico*: Understanding Complexity from Molecules to Ecosystems. Pp 151-176. Springer, Dordrecht 2009.

Santabarbara, S., Heathcote, P., Evans, M.C.V.: Modelling of the electron transfer reactions in Photosystem I by electron tunnelling theory: The phylloquinones bound to the PsaA and the PsaB reaction centre subunits of PS I are almost isoenergetic to the iron–sulfur cluster F_X. – Biochim. Biophys. Acta **1708**: 283-310, 2005.

Satoh, K.: Fluorescence induction and activity of ferredoxin-$NADP^+$ reductase in *Bryopsis* chloroplasts. – Biochim. Biophys. Acta **638**: 327-333, 1981.

Schansker, G., Srivastava, A., Govindjee, Strasser, R.J.: Characterization of the 820-nm transmission signal paralleling the chlorophyll *a* fluorescence rise (OJIP) in pea leaves. – Funct. Plant Biol. **30**: 785-796, 2003.

Schansker, G., Tóth, S.Z., Strasser, R.J.: Methylviologen and dibromorhymoquinone treatments of pea leaves reveal the role of photosystem I in the Chl *a* fluorescence rise OJIP. – Biochim. Biophys. Acta **1706**: 250-261, 2005.

Schreiber, U., Neubauer, C.: O_2-dependent electron flow, membrane energization and the mechanism of non-photochemical quenching of chlorophyll fluorescence. – Photosynth. Res. **25**: 279-293, 1990.

Stirbet, A., Govindjee, Strasser, B.J., Strasser, R.J.: Chlorophyll *a* fluorescence induction in higher plants: Modelling and numerical simulation. – J. Theor. Biol. **193**: 131-151, 1998.

Strasser, B.J.: Donor side capacity of Photosystem II probed by chlorophyll *a* fluorescence transients. – Photosynth. Res. **52**: 147-155, 1997.

Strasser, R.J., Srivastava, A., Govindjee: Polyphasic chlorophyll *a* fluorescence transient in plants and cyanobacteria. – Photochem. Photobiol. **61**: 32-42, 1995.

Strasser, R.J., Stirbet, A.D.: Estimation of the energetic connectivity of PS II centres in plants using the fluorescence rise O-J-I-P - Fitting of experimental data to three different PS II models. – Math. Comput. Simulat. **56**: 451-461, 2001.

Sušila, P., Lazár, D., Ilík, P., Tomek, P., Nauš, J.: The gradient of exciting radiation within a sample affects relative heights of steps in the fast chlorophyll *a* fluorescence rise. – Photosynthetica **42**: 161-172, 2004.

Tomek, P., Lazár, D., Ilík, P., Nauš, J.: On the intermediate steps between the O and P steps in chlorophyll alpha fluorescence rise measured at different intensities of exciting light. – Aust. J. Plant Physiol. **28**: 1151-1160, 2001.

Tóth, S.Z., Schansker, G., Strasser, R.J.: In intact leaves, the maximum fluorescence level (F_M) is independent of the redox state of the plastoquinone pool: A DCMU-inhibition study. –

Biochim. Biophys. Acta **1708**: 275-282, 2005.
Tsimilli-Michael, M., Pêcheux, M., Strasser, R.J.: Vitality and stress adaptation of the symbionts of coral reef and temperature foraminifers probed *in hospite* by the fluorescence kinetics OJIP. – Arch. Sci. **51**: 205-240, 1998.
van Thor, J.J., Geerlings, T.H., Matthijs, H.C.P., Hellingwerf, K.J.: Kinetic evidence for the PsaE-dependent transient ternary complex photosystem I/ferredoxin/ferredoxin:$NADP^+$ reductase in a cyanobacterium. – Biochemistry **38**: 12735-12746, 1999.
Vernotte, C., Etienne, A.-L., Briantais, J.-M.: Quenching of the system II chlorophyll fluorescence by the plastoquinone pool. – Biochim. Biophys. Acta **545**: 519-527, 1979.
Vredenberg, W.J.: A three-state model for energy trapping and chlorophyll fluorescence in photosystem II incorporating radical pair recombination. – Biophys. J. **79**: 26-38, 2000.
Vredenberg, W.J., Bulychev, A.A.: Photo-electrochemical control of photosystem II chlorophyll fluorescence *in vivo*. – Bioelectrochem. **57**: 123-128, 2002.
Vredenberg, W., Prášil, O.: Modeling of chlorophyll *a* fluorescence kinetics in plant cells: derivation of a descriptive algorithm. – In: Laisk, A., Nedbal, L., Govindjee (ed.): Photosynthesis *in silico*: Understanding Complexity from Molecules to Ecosystems. Pp 125-149. Springer, Dordrecht 2009.
Zhu, X.-G., Govindjee, Baker, N.R., deSturler, E., Ort, D.R., Long, S.P.: Chlorophyll *a* fluorescence induction kinetics in leaves predicted from a model describing each discrete step of excitation energy and electron transfer associated with Photosystem II. – Planta **223**: 114-133, 2005.

Appendix

Model reactions: The goal of this paper was to formulate a simple model for the FLR and I_{820} signal. Therefore an effort was concentrated on the electron transport reactions occurring in TM beyond PQ pool as such and not on detailed description of PSII function, including its all known types of heterogeneities. In connection to this, homogeneous populations of all the involved pigment-protein complexes and electron carriers were assumed. Further, to explore an effect of consideration of the electron transport reactions occurring in TM beyond PQ pool as such, no other processes were assumed in the model. Therefore, for example, formation of the light-induced electric potential difference across TM and the electron outflow from PSI to oxygen were not considered in the model. The model considered here describes electron transport reactions occurring in PSII, PQ pool, cyt b_6/f, PC, PSI, Fd, and FNR. A detailed scheme of all reactions considered in the model is shown in Scheme A1. Generally, the demand for simplicity of the model but also the fact that the FLR occurs in time range of tens of μs to hundreds of ms (Fig. 1) restrained electron carriers and reactions between them considered in the model.

For the case of PSII and adjacent space, the S_i-states of OEC, P680, Q_A, Q_B and PQ pool were considered as the electron carriers with following reactions between them (*see* Scheme A1):

1) Light-induced charge separation between P680 and Q_A with rate constant k_{L2} leading to formation of $P680^+$ and Q_A^-. Value of k_{L2} is determined by amount of excitations coming to RCII and concentration of chlorophylls in a sample (Lazár and Pospíšil 1999).

2) Electron donation from S_i-state (i = 0, 1, 2, 3) of OEC to $P680^+$ leading to formation of S_{i+1}-state and P680 with rate constants $k_{0,1}$, $k_{1,2}$, $k_{2,3}$ and $k_{3,0}$ for the S_0-S_1, S_1-S_2, S_2-S_3 and S_3-S_0 transition, respectively.

3) Electron transport from Q_A^- to oxidised or singly reduced Q_B with forward rate constants k_{AB1} and k_{AB2}, respectively. Both these reactions were considered reversible with backward rate constants k_{BA1} and k_{BA2}, respectively.

4) Exchange of doubly reduced (its protonation is not considered explicitly but it is assumed implicitly) Q_B with oxidised PQ molecule from the PQ pool. The exchange was described by reversible second order reaction with forward and backward rate constants k^f_B and k^b_B, respectively.

In the model of PSII reactions, for simplicity OEC was assumed as a separate part which results in existence of 12 model forms (also called state variables) describing the redox state of PSII (*see* Scheme A1) instead of 64 model forms (Lazár and Jablonský 2009). The virtual separation of OEC from PSII, however, might be correct for description of OEC function (Jablonsky and Lazar 2008, Jablonsky *et al*. 2008). Also because of simplicity, the exchange of Q_B^{2-} with PQ molecule from the pool was described by one second order reaction (*e.g*., $P680^+Q_AQ_B^{2-} + PQ \leftrightarrow P680^+Q_AQ_B + PQH_2$) and not by two subsequent reactions (*e.g*., $P680^+Q_AQ_B^{2-} \leftrightarrow P680^+Q_AE + PQH_2$ followed by $P680^+Q_AE + PQ \leftrightarrow P680^+Q_AQ_B$, where E stands for empty Q_B-pocket in PSII). If the latter approach was applied, 16 instead of 12 redox forms would describe the redox state of PSII but this approach does not cause any new effect on the shape of the FLR (Lazár and Jablonský 2009). Moreover, application of the later approach to all related reactions (all reactions involving PQ, PC and Fd) would lead to enormous increase of dimension of the model.

Function of cyt b_6/f was described in the model by means of redox changes of haems *f*, b_L, and b_H in kinetic equilibrium with haem *c* (b_H···*c*) and by means of related electron carriers (PQ, PC, Fd) in adjacent spaces with following reactions between them (*see* Scheme A1):

5) Oxidation of reduced PQ from the pool (its deprotonation is not considered explicitly but it is assumed implicitly) in lumenal side of cyt b_6/f leading to transport of one electron to haem b_L and one electron to haem *f*. This reaction was considered reversible with forward and backward rate constants $k^f_{L,F}$ and $k^b_{L,F}$, respectively.

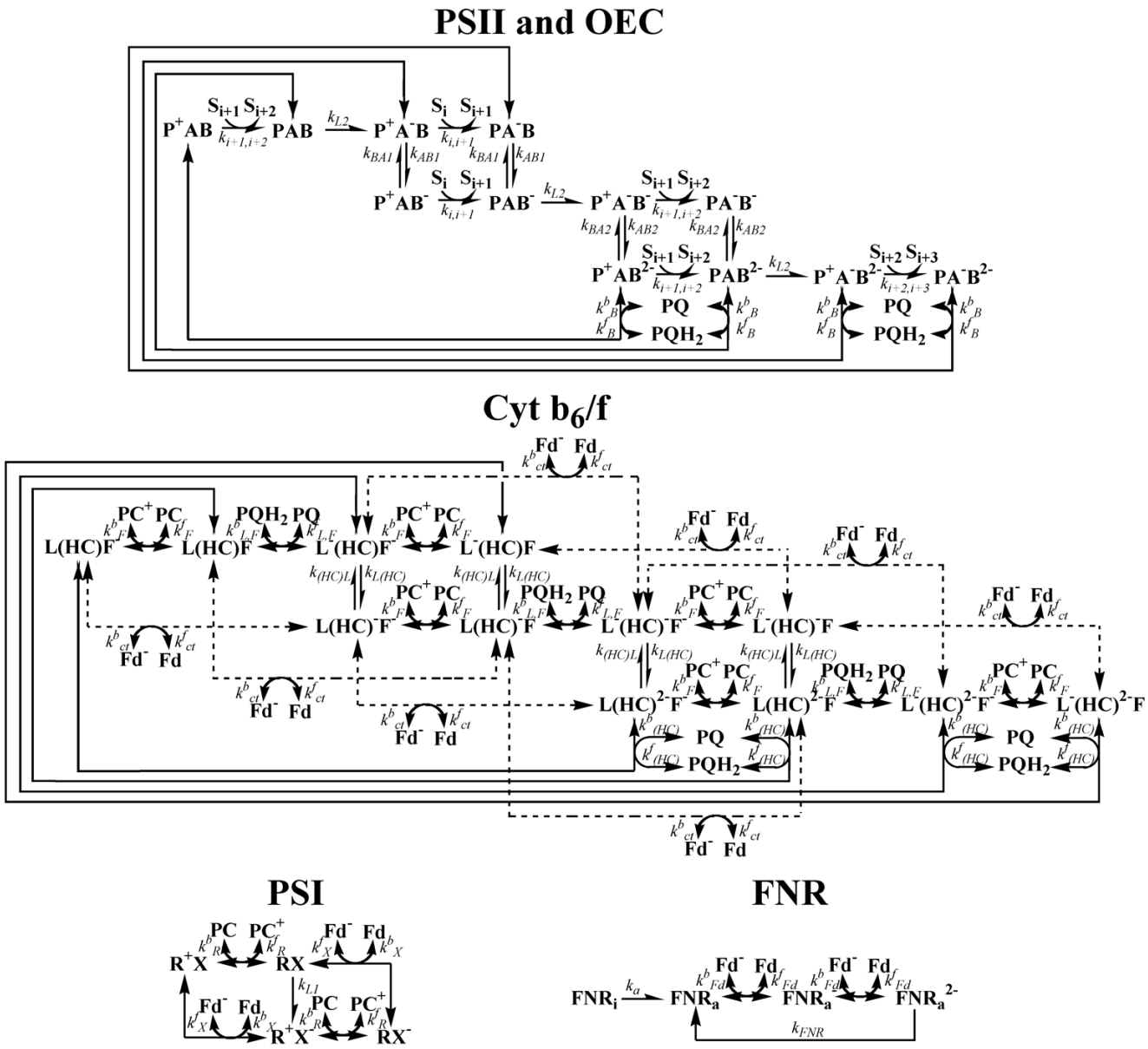

Scheme A1. Scheme of all the reactions considered in the model. Particular parts of the scheme represent reactions related to function of PSII and OEC, cyt b_6/f, PSI and FNR. For a better orientation, reactions in cyt b_6/f, which are related to the CET around PSI, are shown by dashed arrows. In cases where electron carriers are denoted in different way than in the main text (*see* Scheme 1), meaning of the denotation is following: P – P680, A – Q_A, B – Q_B, PQH_2 – reduced and protonated PQ, L – haem b_L, (HC) – haems b_H and *c* in a kinetic equilibrium (b_H···*c*), F – haem *f*, R – P700, X – F_B, FNR_i – inactive FNR, FNR_a – active FNR.

6) Electron transport from b_L^- to oxidised or singly reduced b_H···*c* with the same forward rate constants $k_{(HC)L}$. Both these reactions were considered reversible with the same backward rate constants $k_{L(HC)}$.

7) Reduction of oxidised PQ from the pool (its protonation is not considered explicitly but it is assumed implicitly) in stromal side of cyt b_6/f by $(b_H{}^{\cdots}c)^{2-}$. This reaction was considered reversible with forward and backward rate constants $k^f_{(HC)}$ and $k^b_{(HC)}$, respectively.

8) Oxidation of reduced haem *f* by PC^+. This reaction was considered reversible with forward and backward rate constants k^f_F and k^b_F, respectively.

9) Reduction of oxidised or singly reduced b_H···*c* by Fd^- with the same forward rate constants k^f_{ct}. Both these reactions were considered reversible with the same backward rate constants k^b_{ct}. All these reactions represent the Fd-dependent CET around PSI.

Function of PSI was described in the model very simply by means of redox changes of only P700 and F_B by means of related electron carriers (PC, Fd) in adjacent spaces with following reactions between them (*see* Scheme A1):

10) Light-induced charge separation between P700 and F_B with rate constant k_{L1} leading to formation of $P700^+$ and F_B^-.

11) Reduction of oxidised P700 by PC. This reaction was considered reversible with forward and backward rate constants k^f_R and k^b_R, respectively.

12) Oxidation of reduced F_B by Fd. This reaction was considered reversible with forward and backward rate constants k^f_X and k^b_X, respectively.

Reactions related to function of FNR in the model were as follows:

13) Activation of inactive FNR with rate constant k_a.

14) Reversible electron transport from Fd^- to active oxidised or singly reduced FNR with the same values of the forward and backward rate constants k^f_{Fd} and k^b_{Fd}, respectively.

15) Oxidation of active FNR^{2-} to active FNR with rate constant k_{FNR}. This reaction represents formation of NADPH from $NADP^+$, however, NADPH and $NADP^+$ are not considered explicitly but are assumed implicitly in the model.

Initial conditions and values of rate constants: To simplify and speed up calculations, relative (normalized) amounts instead of absolute concentrations were used. Except of the simulations presented by curves b and c in Fig. 6, the initial conditions (for a dark-adapted state) for all the simulations were: 75 and 25% of OEC being in the S_1- and S_0-state, respectively, Q_A and Q_B fully oxidised, P680 fully reduced, a half of PQ molecules reduced and a half of them oxidised, haems b_L, (b_H ··· c), and f fully oxidised, PC and P700 fully reduced, F_B and Fd fully oxidised, and FNR fully inactive. Considering ratio of particular pigment-protein complexes and electron carriers assumed in the model OEC:PSII:PQ:cyt b_6f:PC:PSI:Fd:FNR = 1:1:5:1:3:1:3:3 and denotation of the model forms as used in Scheme A1, the initial conditions can be rewritten as: $[S_1]_0 = 0.75$, $[S_0]_0 = 0.25$, $[PAB]_0 = 1$, $[PQ]_0 = 2.5$, $[PQH_2]_0 = 2.5$, $[L(HC)F]_0 = 1$, $[PC]_0 = 3$, $[RX]_0 = 1$, $[Fd]_0 = 3$, $[FNR_i]_0 = 3$ with all other model forms in Scheme A1 being zero initially.

Table A1. Values of the rate constants used in the model. Because of the used normalization, all rate constants have dimension s^{-1}.

Rate constant	Value	Reference or note
k_{L2}	4000	Lazár (2003)
$k_{0,1}$	20000	
$k_{1,2}$	10000	
$k_{2,3}$	3330	
$k_{3,0}$	1000	
k_{AB1}	3500	
k_{BA1}	175	
k_{AB2}	1750	
k_{BA2}	35	
k^f_B	250	
k^b_B	250	
$k^f_{L,F}$	100	estimate
$k^b_{L,F}$	10	
$k_{(HC)L}$	2300	Crofts and Wraight
$k_{L(HC)}$	7	(1983)
$k^f_{(HC)}$	100	estimate
$k^b_{(HC)}$	10	
k^f_F	100	
k^b_F	10	
k^f_{ct}	100	
k^b_{ct}	100	
k_{L1}	200	
k^f_R	100	
k^b_R	10	
k^f_X	100	
k^b_X	10	
k_a	0.01	
k^f_{Fd}	5	
k^b_{Fd}	5	
k_{FNR}	220	van Thor *et al*. (1999)

Usage of the relative amounts of the model forms leads to a change of the values and dimensions of some of the rate constants. Rate constants of the first order reactions retain their original values and dimensions (s^{-1}). However, rate constants of the second order reactions have after normalization much smaller values and the same dimensions as the first order rate constants (s^{-1}). For the rationale of the rescaling, *see* Kroon and Thoms (2006). Values of the rate constants (after the normalization) used in the model are listed in Table A1. Values of some of the rates constant were found by trail-and-error approach (Lazár *et al*. 2005) to obtain a satisfactory shape of the FLR and I_{820} signal curves. However, the values of the rate constants are "comparable" with values of "similar" rate constants in the model (k^f_B, k^b_B) and hence represent a reasonable estimate. Further, without going into details, after back re-calculation of the normalized values of the rate constants, the original values are in many cases comparable with the values found in literature.

The value of k_{L1} (reaction 10) should be, as in the case of PSII (*see* reaction 1), determined by amount of excitations coming to reaction centre of PSI (RCI) and concentration of Chls in a sample. However, a value of k_{L1} comparable with the value of k_{L2} did not lead to correct simulation of the I_{820} signal ($P700^+$ started to accumulate before 1 ms leading to a wide minimum of the I_{820} signal). Also an effort to reduce the soon accumulation of $P700^+$ by increasing the value of the forward rate constant of $P700^+$ reduction by reduced PC (k^f_R) or less directly by increasing the value of the forward rate constant of CET (k^f_{ct}) did not lead to an improvement. Hence, the value of k_{L1} was set by the trail-and-error approach to 200 s^{-1}.

DBMIB- and MV-treatments and dependence on light intensity: To simulate the effect of DBMIB- or MV-treatments, values of $k^f_{L,F}$ and $k^b_{L,F}$ were set to 0 (DBMIB case) or a pool of MV (with fixed relative amount 10) irreversibly accepted electrons from reduced F_B with a value of rate constant of 100 s^{-1} (MV case). For the simulations of the light intensity dependencies, the values of k_{L2} and k_{L1} were percentually decreased with respect to the values of k_{L2} and k_{L1} listed in Table A1, which represent 100%.

Definition of fluorescence and I_{820} signal: Fluorescence signal during the FLR was calculated from time courses of model forms. A sum of all model forms with reduced Q_A, $\Sigma[Q_A^-](t)$, was used for calculation of unquenched fluorescence signal, $F_{unq}(t)$, with respect to assumed energetic connectivity between PSIIs (Joliot and Joliot 1964) as:

$$F_{unq}(t) = ((1 - p) \times \Sigma[Q_A^-](t)) / (1 - p \times \Sigma[Q_A^-](t)),$$

where p (= 0.55) is the connectivity parameter. From the unquenched fluorescence, fluorescence quenched by oxidised PQ molecules (Vernotte *et al*. 1979), $F_q(t)$, was calculated as:

$$F_q(t) = F_{unq}(t) / (1+ ((a + (\Sigma[Q_A^-](t) \times b)) \times [PQ](t))),$$

where [PQ](t) is the amount of oxidised PQ molecules and the constants a (= 1/45) and b (= 4/63) were calculated (assuming 10 and 30% quenching of F_0 and F_M, respectively, and 5 PQ molecules) as described in details in Stirbet *et al*. (1998). Time courses of the quenched fluorescence signal ($F_q(t)$) were used for the calculations of the relative variable fluorescence as presented in all figures. However, existence of the fluorescence quenching by oxidised PQ molecules in leaves was questioned (Tóth *et al*. 2005), though it can be observed in thylakoid preparations of different integrity (Kurreck *et al*. 2000).

The I_{820} signal was calculated as:

$$I_{820}(t) = 10^{-(A_{PC^+}(t) + A_{\Sigma P700^+}(t))},$$

using

$$A_{PC^+}(t) = d \times c \times \varepsilon_{PC^+} \times [PC^+](t)$$

and

$$A_{\Sigma P700^+}(t) = d \times c \times \varepsilon_{P700^+} \times \Sigma[P700^+](t),$$

where d is the path length, c is the molar concentration of RCI, ε_{PC^+} and ε_{P700^+} are particular molar extinction coefficients and $[PC^+](t)$ and $\Sigma[P700^+](t)$ are time courses of oxidised PC and sum of oxidised P700 (sum of R^+X and R^+X^- model forms), respectively. The thickness of the leaf (assumed to be 0.01 cm) might be considered as the path length but because of a scatter of the light in scattering medium, such as leaf is (*e.g*., Oja *et al*. 2004), the path length is prolonged. For an assumed standard green leaf with concentration of about 30 μg (Chls *a* and *b*) cm^{-2} (Ilík *et al*. 2000), the prolongation of the path length was found by factor 2.75 (McClendon and Fukshansky 1990). Therefore, the path length was assumed to be 0.0275 cm. To calculate the molar concentration of RCI the standard green leaf was considered that corresponds to concentration of 3 g (Chls *a* and *b*) l^{-1}, assuming the thickness of a leaf, that results in concentration of about 3.3 mM (Chls *a* and b), assuming average molecular molar mass of Chls (*a* and *b*) to be 900 g mol^{-1}. Assuming 1/1 ratio for PSII/PSI and 250 and 170 Chls (*a* and *b*) to be associated with PSII and PSI, respectively, it results in

concentration of 7.85 μM RCI. The used molar extinction coefficients are 1590 M^{-1} cm^{-1} for PC^+ and 10300 M^{-1} cm^{-1} for $P700^+$ as determined for single wavelength (810 nm) measuring setup and spinach chloroplasts by Kirchhoff *et al.* (2004).

Separate contributions of oxidised PC and sum of oxidised P700 to overall I_{820} signal (Figs. 3*B*, 4*A,B*) were calculated as:

$$I_{820,PC^+}(t) = 10^{-A_{PC^+}(t)}$$

and as:

$$I_{820,\Sigma P700^+}(t) = 10^{-A_{\Sigma P700^+}(t)},$$

respectively. However, such separation of the contributions by oxidised PC and oxidised P700 into two independent signals is only hypothetical and is not justified for real sample because the action of oxidised PC an oxidised P700 on measured 820 nm-transmittance signal is always simultaneous and affects each other and cannot be mutually separated.